Reply to report of reviewer #1
"Errors in satellite-based global horizontal irradiance retrievals due to three-dimensional cloud-radiation interactions by Wiltink et. al."

bold italic font = reviewer's comment
regular font = authors' reply
red regular font = original text in the manuscript
blue regular font = newly added or updated text in the manuscript

---

General comments

This study evaluates errors in satellite retrievals of global horizontal irradiance (GHI) due to three-dimensional (3D) cloud-radiation interactions at different spatial resolutions (from fine (50 m) to coarse resolutions (12.4 km)). This is achieved by utilizing two shallow-cumulus Large Eddy Simulations (LES) cloud fields, alongside retrieval algorithms and both 3D and 1D radiative transfer framework to perform a comprehensive study via a 1D/3D GHI retrieval vs 1D/3D GHI reference pathway approach, and mapping of differences to plane parallel approximation (PPA), independent pixel approximation (IPA) and residual biases. They show that at fine spatial resolutions current retrieval algorithms assuming the IPA prove to be insufficient to accurately resolve heterogeneous cloud conditions and emphasize the need to develop 3D RT parameterizations and corrections for GHI retrievals.

The work is well motivated, interesting, and the manuscript is mostly well written. There are a few areas where I think more examples and explanations are needed. For example, the study was mostly based on nadir viewing ($\theta = 0^\circ$) to avoid parallax error, even though geostationary satellites viewing zenith observations over mid-latitudes are typically off-nadir. The study also includes slant-view case ($\theta = 70^\circ$) and discusses parallax induced smoothing, but the operational message ("The current generation of geostationary satellites already resolves these finer spatial scales in which IPA-related errors dominates") partly depends on typical viewing conditions. It would be interesting to add one intermediate viewing zenith angle (e.g., 35 - 45°) to bridge between overhead (0°) and extreme (70°) view zenith. Also, since this study is based on two cloud fields of the same cloud type (shallow cumulus clouds), care should be taken to draw conclusions objectively from the results. These are all minor concerns and are stated in my specific comments below. I congratulate the authors for this great work and, after addressing these remarks, I recommend prompt publication in ACP.

We thank the reviewer for taking the time to review our document and provide constructive feedback. We agree that caution is required when generalising, for instance, to other cloud types. This study focuses on two highly variable cumulus cloud fields; hence, 3D cloud-radiation interactions are likely to be less prominent under more homogeneous conditions. However, since this has not been investigated in the current study, it should be mentioned more clearly. We will clarify this in the Conclusions and Outlook section:

P29 L555: Two highly variable [...] are studied. Since this study only presents results for two highly variable cumulus cloud fields, future studies should clarify how the presented results generalise to other cloud conditions.

Moreover, since reviewer #2 also expressed concern about remaining uncertainties and generalisability, we have decided to include an additional discussion section addressing these topics. For further details, please see our reply

to reviewer #2.

Finally, please find our response to the point raised about intermediate viewing angles in the corresponding specific comment below.

Specific comments

L97: Do both cloud scenarios have the same cloud top height (CTH) of 6.4 km? If not, state the CTH of each cloud scene and briefly explain how the CTH and cloud base height (CBH) of the two cloud fields were obtained.
The 6.4 km mentioned in the article refers to the domain top height in the LES simulations and does not represent the cloud top height. The actual cloud top (and bottom) heights are variable depending on the liquid water content of the grid cells from the LES output. To indicate cloud height, we will mention the domain-averaged cloud-top and cloud-bottom heights (excluding clear-sky pixels) for both scenes in the revised manuscript. The cloud top and bottom heights are derived for each column as the highest/lowest level where LWC > 0 kg m^{-3}, respectively.

Page 4, L103: The cloud cover [..] is 22%. The cloud base and cloud top heights, as determined from the lowest and highest level with a non-zero liquid water content, vary over the domain. The domain-averaged cloud base and top heights are 1550 m and 1867 m, respectively.
Page 4, L105 Compared to [..] 64 %. Compared to scene 1, the domain-averaged cloud base and cloud top are slightly higher, at 1884 m and 2126 m, respectively.

L113: Reference this study: https:/doi.org/10.1029/2022JD036822 and include it in the discussion. Ambient aerosols have been shown to have a significant impact on the 3D radiative effect of cumulus scenes such as those considered in this work.
We thank the reviewer for bringing this publication to our attention. We will include the reference in the new Section discussing generalisability and remaining uncertainties. See reply to reviewer #2.

L118-119: Provide a justification for rounding the scene cloud droplet effective radii to their nearest integer values. The authors referred to Sect 3.1 where we see the range of droplet radii for MONKI simulations as 3 to 22 µm in 1 µm steps, but no satisfactory justification was made.
The rounding of cloud droplet effective radii was done for practical considerations related to the simulation of synthetic TOA reflectances. To run the MONKI Monte Carlo code, for each droplet size, files containing information on scattering properties are required (e.g., scattering phase functions). These files were generated with the Meerhof Mie Program. As long as the scattering files are available, MONKI can also simulate reflectances for intermediate effective cloud droplet radii. However, including a wider range of droplet sizes in a single simulation reduces computational performance. Since the simulations were already computationally intensive, we have decided not to further increase the number of cloud droplet effective radii.

We will add a justification to the document:
Page 6, Line 145: The range [..] is 3 to 22 µm in steps of 1 µm. This step size was used since including droplet sizes with smaller steps would make the MONKI simulations computationally unfeasible.

Fig. 1: I really like this figure. It captures the descriptions of the methods in the text. Two comments:

1. ***The rectangle in the topmost row showing the reflectance output from MONKI (3D), it will be helpful to include "(3D)" to the VIS/NIR reflectances. This would aid swift visualization that the reflectances here are from 3D RT and readers can grab the big picture by just looking at the figure.***
2. ***Try to indicate that the CPP-SICCS in the first two rows are based on plane-parallel atmosphere and the different columns are independent. Like include "(1D RT theory)" or "1D"***

We thank the reviewer for these suggestions. The figure has been updated based on the above-mentioned comments.

L164-167: cloud mask is generated based on the liquid water path from the LES data based on LES LWP > 0, while retrieved optical depth can return small non-zero τ even in clear pixels, and a separate τ> 0 condition is also mentioned for cloudy masking. Because much of the mechanism relies on pixels being (mis)classified as cloudy/clear (especially enhancement/shading), inconsistencies here could affect residual attribution. What is the mismatch frequency between (LWP> 0) and (retrieved τ > 0) at each resolution (or at least at 50 m and one coarser scale)? Show that the main conclusions are not driven by classification artifacts. Consider reporting a sensitivity where the retrieval uses the retrieved τ threshold consistently for SICCS cloudy/clear (even if only for one scenario).

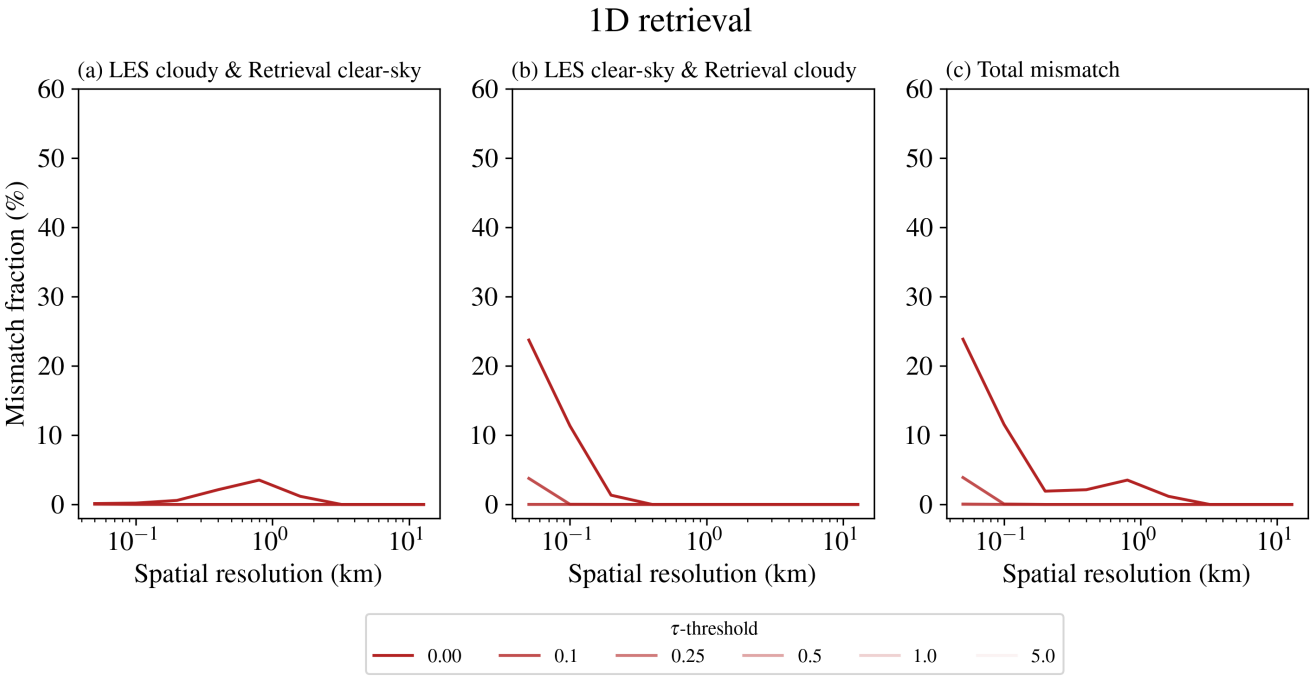

Figure R1.1: Mismatch fractions between cloud masks for the 1D retrieval: (a) LES cloudy and retrieved clear-sky; (b) LES clear-sky and retrieved cloudy; (c) total mismatch error. Results are shown for the default scenario, where apart from the standard $\tau = 0$ threshold to separate clear and cloudy pixels also other τ thresholds are included.

Two cloud masks are indeed used in this study, and they are not identical. The LES cloud mask is used throughout the paper, but the retrieval has its own cloud mask based on the inferred cloud optical thickness. We have performed an analysis of the mismatch between these cloud masks for the 1D and 3D retrieval. The sensitivity to hypothetical τ-thresholds larger than zero is also analysed.

1D retrieval

The misclassification for the 1D retrieval remains limited. The mismatch fraction for pixels being cloudy in the LES cloud mask but clear sky in the retrieval cloud mask is only 0.15 % at the finest resolution (Fig R1.1a). For pixels with a very thin optical depth between 0 and 0.05, spatial averaging does increase the mismatch to 4 % around 800 m resolution. However, if only misclassification for retrieved optical depths above 0.1 are considered, the mismatch error does not increase with coarser spatial resolutions.

The mismatch where the LES cloud mask is clear-sky and the retrieval cloud mask is cloudy is slightly larger (Fig R1.1b). This is mainly due to residual noise in the synthetic MONKI simulations. Note that the optical depth of these misclassified pixels is very low. At the finest resolution, the misclassification is below 0.1% in case only misclassified pixels with an optical depth larger than 0.25 are considered. With such small optical depths being retrieved, consequently, GHI errors will remain limited.

3D retrieval

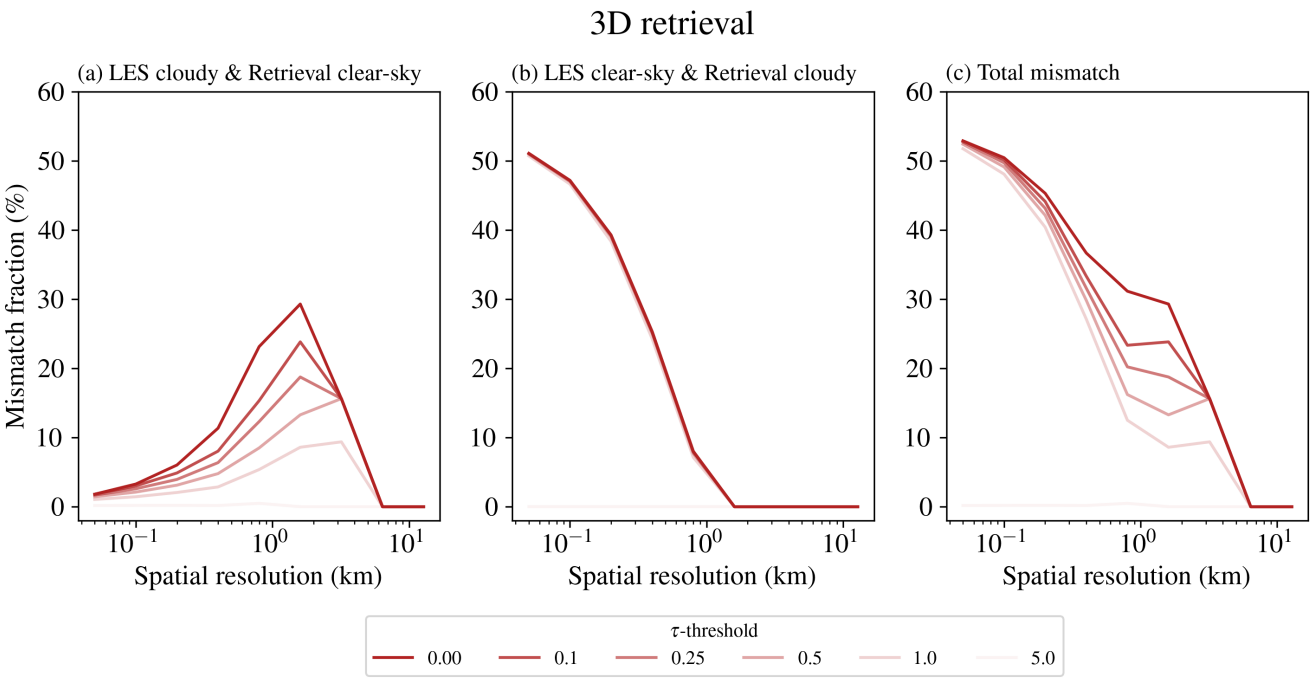

Figure R1.2: Same as Figure R1.1, but now for the 3D retrieval.

In the 3D retrieval, misclassification errors are much more prevalent, which is expected as a result of 3D cloud-radiation interactions. The misclassification of pixels where the LES cloud mask is cloudy and the retrieval cloud mask is clear sky (Fig. R1.2a) is below 2 % at the finest spatial resolution but does increase over 30 % around a 1.6 km spatial resolution. Note that, with spatial averaging, the LES cloud mask becomes increasingly cloudy as more pixels receive an LWP greater than 0. In the retrieval cloud mask, which is based on reflectances, spatial averaging of cloud-shaded pixels with cloudy pixels can cause cloudy pixels to become clear-sky, thus introducing a mismatch.

Finally, we focus on the misclassification for pixels that are clear-sky in the LES cloud mask but cloudy in the retrieval cloud mask (Fig. R1.2b). As it turns out, at the finest spatial resolution, about half of the pixels are misclassified. This can be attributed to errors caused by irradiance enhancement in clear-sky pixels. At coarser resolutions, errors due to irradiance enhancement become less prominent, and the misclassification disappears.

All in all, the misclassification of clear/cloudy pixels in the cloud mask based on reflectance is one of the causes of retrieval errors due to 3D radiative effects. We have decided to exclude the above two figures (R1.1 and R1.2) in the main manuscript. The mechanisms (shading and irradiance enhancements) explaining the trends of figures R1.1 and R1.2 are already described in the manuscript. For instance, in Figure 9 of the manuscript, the relation between reflectance and errors in irradiance enhancement and shading are discussed.

L194: As mentioned in the general comments above, can you include an experiment for intermediate viewing zenith angle (e.g., 35 - 45°) to bridge between overhead (0°) and extreme (70°) view zenith, showing how these compares to the current results. This can be discussed in Section 5.3 L514 to L546.

Initially, we performed the simulation with an extreme viewing zenith angle of 70° to illustrate the possibility of positive clear-cloudy mixing errors. Based on the reviewer's feedback, an additional simulation with a viewing zenith angle of 40° is performed.

The results for VZA=40° will be included in a revised Figure 17. The new scenario will also be added to Table 1. Furthermore, the results will be discussed in Section 5.2, as follows.

Viewing geometry sensitivity

With the relation between clear-cloudy mixing and viewing geometry pointed out in Sect. 5.1, here the scenarios are presented for viewing angles of 40°, and 70°. By evaluating Figure 16 for these two scenarios (also see Table 1), either limited ($\theta = 40°$) or positive ($\theta = 70°$), clear-cloudy mixing biases are expected.

First, for both slanted viewing angles, the PDF of the 1D retrieval is again dominated by high probability densities for the clear-sky pixels (dotted lines, Fig. 17a,d). For the retrieval based on 3D reflectances, clearer deviations are apparent compared to the default scenario. The peak in probability density corresponding to the clear-sky pixels that are incorrectly retrieved as cloudy is closer to the actual clear-sky value than for the default scenario (Compare solid lines of Fig. 17a,d to Fig. 7e). This indicates a smaller error due to irradiance enhancement as the viewing angle increases. Although the peak itself is narrower, in the scenario where $\theta = 70°$, the peak's base is broader than in the default scenario, which we attribute to parallax.

Parallax is the shift between the actual position (from the LES data) and apparent (retrieved) position of an observed object (i.e. clouds). Until this section, all retrievals were performed for nadir viewing angles for which there is no parallax. Slanted viewing results in a shift of the projected location of the clouds in the direction away from the observer. The magnitude of parallax depends on the height of the cloud and the viewing angle. Larger displacements occur for higher clouds or at larger viewing zenith angles. For the retrievals with slanted viewing angles, each pixel will have variable parallax due to variations in cloud occurrence and vertical structure. As a result, clouds that are projected onto a single pixel at nadir viewing might be projected onto multiple pixels at a higher θ, leading to smoother reflectances. If reflectances are smoothed, the retrieved cloud edges become less sharp, resulting in a smoother transition from clear to cloudy in the PDF for retrieved GHI. Due to smoothing, the retrieved cloud fraction effectively increases (not shown). Another effect of the smoothing is that both the fraction of irradiance-enhanced and cloud-shaded pixels is reduced, also reducing the retrieval error due to shading and irradiance enhancement. On the other hand, parallax does introduce an additional mismatch, as clear-sky pixels will be incorrectly classified as cloudy by the retrieval.

At a θ of 40° the change in domain-averaged GHI remains limited (triangular markers in Fig. 17b). Meanwhile, for $\theta = 70°$, an increase in domain-averaged GHI is observed for the 1D retrieval as the resolution gets coarser (triangular markers in Fig. 17e). Both observations are as expected because with a θ of 40°, the clear-cloudy mixing bias remains limited and for $\theta = 70°$, even a positive GHI bias is expected due to clear-cloudy mixing (see Fig. 16).

For the retrievals based on 3D reflectances (cross markers in Fig. 17b,e), towards coarser resolutions, there is an increase in domain-averaged GHI as a result of the increase in relative importance of the retrieval error due to shading over the retrieval error due to irradiance enhancement. However, at coarser spatial resolutions, for both viewing angles, no decrease in domain-averaged GHI is observed as was the case for the default scenario of scene 1. At these coarser resolutions, the influence of irradiance enhancement and shading are limited. Moreover, for these geometries, at coarser resolutions, changes due to clear-cloudy mixing are limited as well (see 1D retrieval 17b,e), and therefore GHI remains unchanged towards even coarser resolutions.

Finally, for the biases (Fig. 17c,f), the IPA-related biases are identical to the default scenario. Since the averaged GHI of the references is constant with resolution, the PPA-related bias follows the same trend as the 1D retrieval. Next, both at a θ of 40° and a θ of 70° a positive trend in residual bias is observed if spatial resolution gets coarser. However, contrary to the scenarios with a nadir view and varying solar zenith angles, albedo, and cloud cover, for the scenario with a θ of 70°, the residual bias remains negative at all spatial resolutions. Overall, for this viewing angle, this results in a negative total bias which vanishes for spatial resolutions of 1.6 km and coarser. Interestingly, at a θ of 40° the total bias is minimal, already at a spatial resolution of 0.2 km. For most other scenarios the total bias reaches its minimum at spatial resolution between 1 and 3 km. What the scenario of $\theta = 40°$ indicates is that the observed minimal biases around 1 km, are not a general rule but heavily depend on the present geometry.

The caption of Figure 17 will be updated to the following.
PDFs of GHI at 0.05 km (a,d) and resolution dependence of domain-averaged GHI (b,e) for the retrieval and reference based on 1D or 3D RT and the biases separated into the contributions due to the PPA, IPA and residual

errors (c,f). The scenario is scene 1 with $\theta = 40°$ (a,b,c), $\theta = 70°$ (d,e,f) and $\phi = 124°$. The solar position is equal to the default scenario with $\theta_0 = 51°$ and $\phi_0 = 184°$.

L525 - 529: "The magnitude of parallax depends on the height of the cloud and the viewing angle." One suggestion is to include a figure of the cloud top height and cloud base height for clouds, this would allow the readers to see the CTH distribution and might envisage how shadowing of one cloud can affect its neighbor, depending on the solar-view geometry.

We have created a figure (see Fig. R1.4, below) illustrating the cloud top height and the degree of parallax displacement for two viewing angles. While it does illustrate the effect of parallax, we are not fully convinced it fits the scope of the current article. In previous work (i.e. Wiltink et al., 2025), we conducted a more in-depth analysis of the effect of parallax on retrieval accuracy, including its relation to cloud top height. Moreover, in Figure 9 of Miller et al. (2018), the relation between zenith angle, cloud top height and parallax is nicely illustrated. Therefore, we have decided not to include this figure in the manuscript; the two references mentioned above will be added after this sentence at l. 525.

P27 l. 525 The magnitude of parallax depends on the height of the cloud and the viewing angle (Miller et al., 2018; Wiltink et al., 2025).

Technical corrections

L7: Abstract indicates resolution range considered as 0.05 to 12.4 km (as well as L80 and L553), while in L207 the largest resolution was stated as 12.2 km. Please standardize (12.2 vs 12.4).
We thank the reviewer for pointing out this inconsistency. In fact, both 12.2 km and 12.4 km are incorrect as the coarsest resolution. The correct value should be 12.8 km. This is because the spatial resolution was doubled in 8 steps from 0.05 to 12.8 km. The values will be been updated throughout the document.

L103: The Solar zenith angle for scene 1 is given as 50.53° but Table 1 and elsewhere often uses 51°. This is okay but clarify rounding.
The value of 50.53° for the solar zenith angle (as well as 184.2° for the solar azimuth angle) is the more precise value used in this study. For clarity, we will round these values to the nearest whole number, which we now also clarify in the text.

Page 4, L103: At 12 UTC the Sun is approximately south [...] a solar zenith angle of 50.53°. In the remainder of the article, these values will be presented rounded to the nearest integer.

L152: Replace "which would additional uncertainties" with "which would cause additional uncertainties"
The text will be modified accordingly.

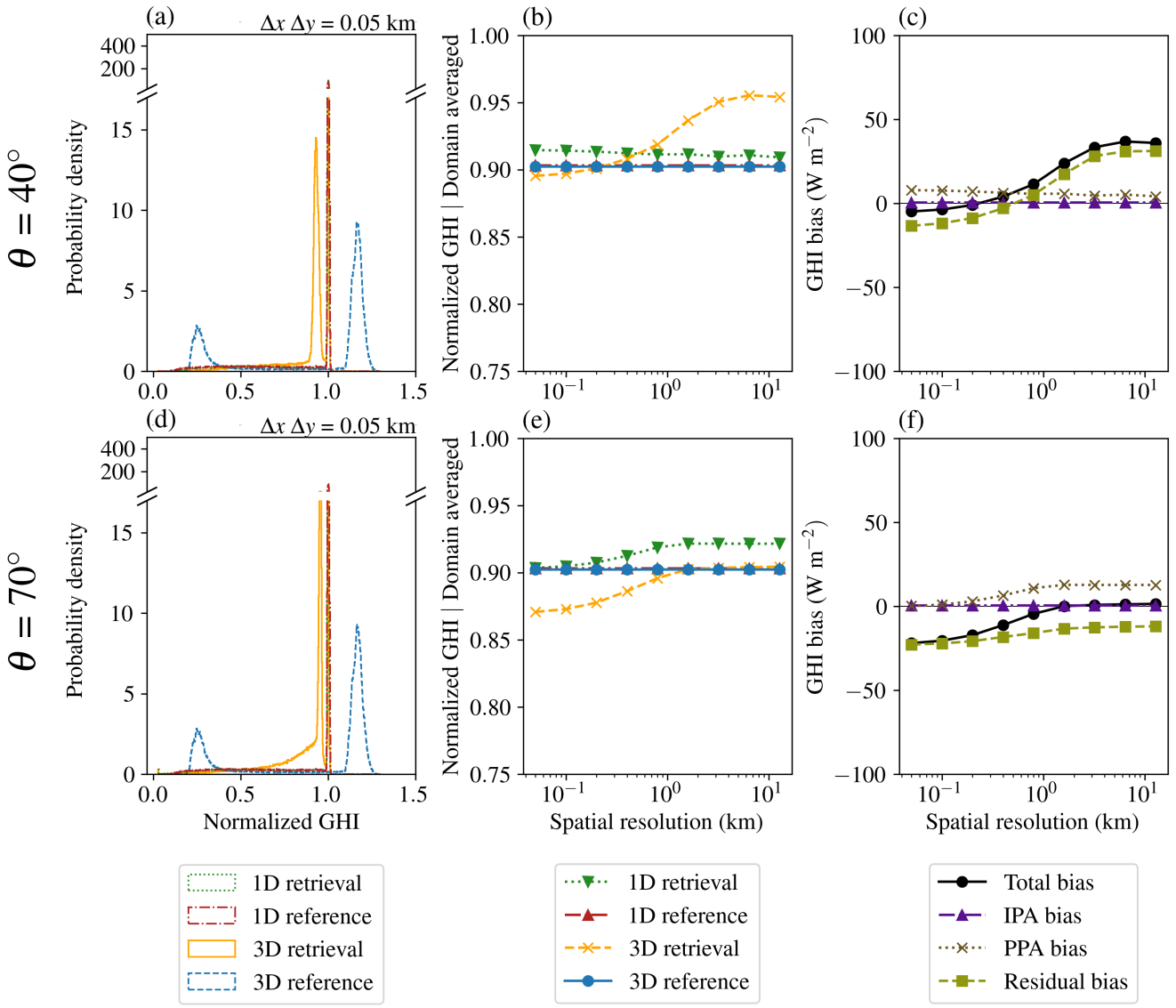

Figure 17: PDFs of GHI at 0.05 km (a,d) and resolution dependence of domain-averaged GHI (b,e) for the retrieval and reference based on 1D or 3D RT and the biases separated into the contributions due to the PPA, IPA and residual errors (c,f). The scenario is scene 1 with $\theta = 40°$ (a,b,c) or $\theta = 70°$ (d,e,f) and $\phi = 124°$. The solar position is equal to the default scenario with $\theta_0 = 51°$ and $\phi_0 = 184°$.

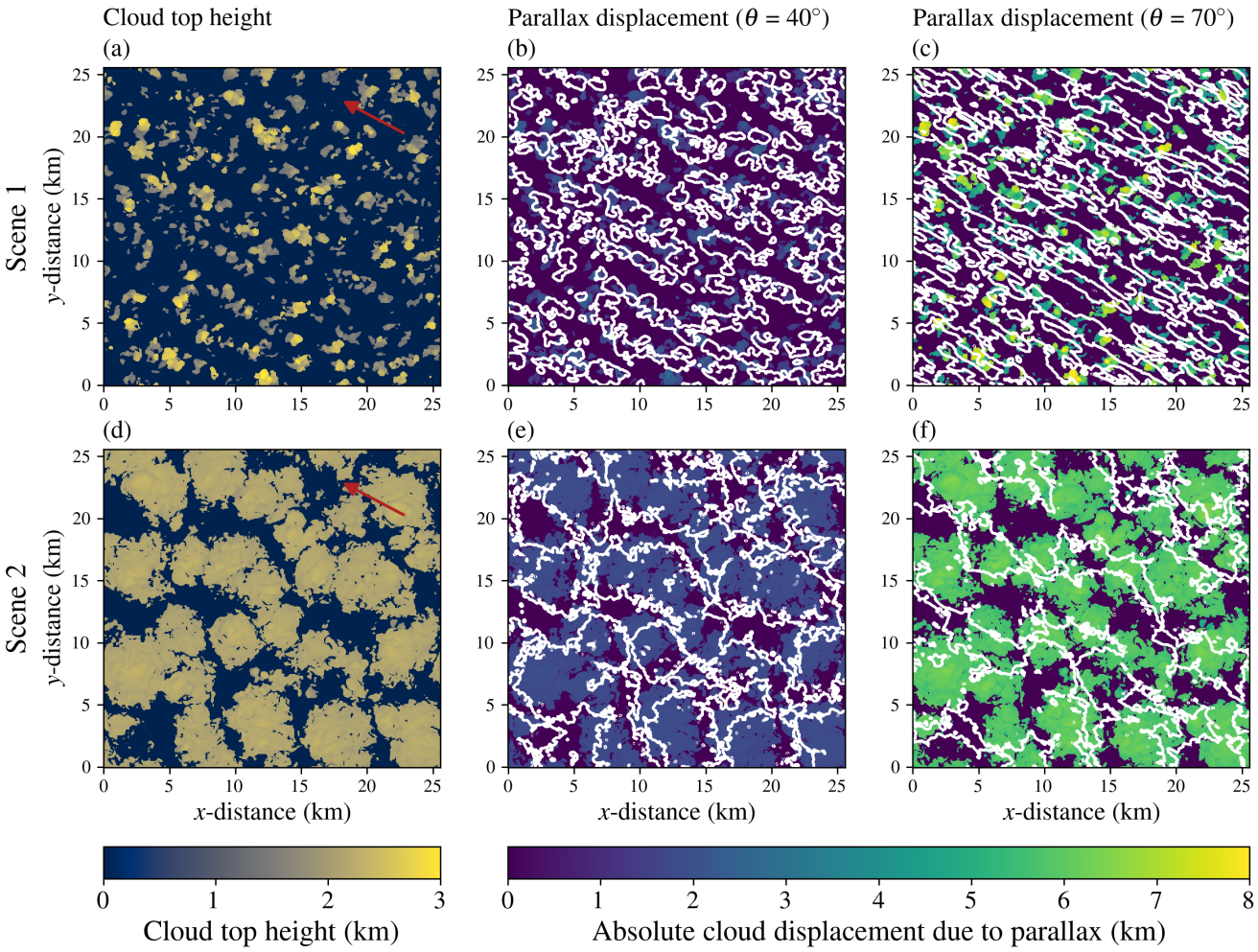

Figure R1.4: Cloud top height of scene 1 (a) and scene 2 (d) along with the absolute cloud displacement due to parallax at viewing angles of 40° and 70° for scene 1 (b,c) and scene 2 (e,f), respectively. The white contours (b,c,e,f) indicate the cloud position uncorrected for parallax. The red arrows in (a,d) indicate the satellite viewing direction.

References

Miller, S. D., Rogers, M. A., Haynes, J. M., Sengupta, M., and Heidinger, A. K.: Short-term solar irradiance forecasting via satellite/model coupling, Solar Energy, 168, 102–117, https://doi.org/10.1016/J.SOLENER.2017.11.049, 2018.

Wiltink, J. I., Deneke, H., van Heerwaarden, C. C., and Meirink, J. F.: Evaluating parallax and shadow correction methods for global horizontal irradiance retrievals from Meteosat SEVIRI, Atmospheric Measurement Techniques, 18, 3917–936, https://doi.org/10.5194/amt-18-3917-2025, 2025.